Received: 7 October 2022 | Accepted: 14 October 2022

DOI: 10.1002/ece3.9469

RESEARCH ARTICLE

Ecology and Evolution Open Access WILEY

Segregational instability of multicopy plasmids: A population genetics approach

J. Carlos R. Hernandez-Beltran[1,2] | Verónica Miró Pina[3,4,5] | Arno Siri-Jégousse[5] | Sandra Palau[5] | Rafael Peña-Miller[1] | Adrián González Casanova[6]

[1]Systems Biology Program, Center for Genomic Sciences, Universidad Nacional Autónoma de México, Cuernavaca, Mexico

[2]Department of Microbial Population Biology, Max Planck Institute for Evolutionary Biology, Plön, Germany

[3]Centre for Genomic Regulation (CRG), The Barcelona Institute of Science and Technology, Barcelona, Spain

[4]Universitat Pompeu Fabra (UPF), Barcelona, Spain

[5]Departamento de Probabilidad y Estadística, Instituto de Investigación en Matemáticas Aplicadas y en Sistemas, Universidad Nacional Autónoma de México, Cuernavaca, Mexico

[6]Instituto de Matemáticas, Universidad Nacional Autónoma de México, Cuernavaca, Mexico

Correspondence
Adrián González Casanova, Instituto de Matemáticas, Universidad Nacional Autónoma de México, Cuernavaca, Mexico.
Email: adriangcs@matem.unam.mx

Funding information
CONACYT Mexico, Grant/Award Number: A1-S-14615 and A1-S-32164; Universidad Nacional Autónoma de México, Grant/Award Number: IA103820, IN101722 and IN209419

Abstract

Plasmids are extra-chromosomal genetic elements that encode a wide variety of phenotypes and can be maintained in bacterial populations through vertical and horizontal transmission, thus increasing bacterial adaptation to hostile environmental conditions like those imposed by antimicrobial substances. To circumvent the segregational instability resulting from randomly distributing plasmids between daughter cells upon division, nontransmissible plasmids tend to be carried in multiple copies per cell, with the added benefit of exhibiting increased gene dosage and resistance levels. But carrying multiple copies also results in a high metabolic burden to the bacterial host, therefore reducing the overall fitness of the population. This trade-off poses an existential question for plasmids: What is the optimal plasmid copy number? In this manuscript, we address this question by postulating and analyzing a population genetics model to evaluate the interaction between selective pressure, the number of plasmid copies carried by each cell, and the metabolic burden associated with plasmid bearing in the absence of selection for plasmid-encoded traits. Parameter values of the model were estimated experimentally using *Escherichia coli* K12 carrying a multicopy plasmid encoding for a fluorescent protein and $bla_{\text{TEM-1}}$, a gene conferring resistance to β-lactam antibiotics. By numerically determining the optimal plasmid copy number for constant and fluctuating selection regimes, we show that plasmid copy number is a highly optimized evolutionary trait that depends on the rate of environmental fluctuation and balances the benefit between increased stability in the absence of selection with the burden associated with carrying multiple copies of the plasmid.

KEYWORDS
experimental microbiology, plasmid dynamics, population genetics

TAXONOMY CLASSIFICATION
Genetics, Theorectical ecology

J. Carlos R. Hernandez-Beltran and Verónica Miró Pina contributed equally to this work

1 | INTRODUCTION

Prokaryotes transfer DNA at high rates within microbial communities through mobile genetic elements such as bacteriophages (Chen et al., 2018), transposons (Chen & Dubnau, 2004), or extrachromosomal DNA molecules known as plasmids (Funnell & Phillips, 2004). Crucially, plasmids have core genes that allow them to replicate independently of the chromosome but also encode for accessory genes that provide their bacterial hosts with new functions and increased fitness in novel or stressful environmental conditions (Groisman & Ochman, 1996). Plasmids have been widely studied due to their biotechnological potential (Alonso & Tolmasky, 2020) and their relevance in agricultural processes (Pemberton & Don, 1981), but also because of their importance in clinical practice since they have been identified as significant factors contributing to the current global health crisis generated by drug-resistant bacterial pathogens (San Millan, 2018).

Although the distribution of plasmid fitness effects is variable and context dependant (Alonso-del Valle et al., 2021), it is generally assumed that in the absence of selection for plasmid-encoded genes, plasmids impose a fitness burden on their bacterial hosts (Baltrus, 2013; San Millan & Maclean, 2017). As a result, plasmid-bearing populations can have a competitive disadvantage compared with plasmid-free cells, thus threatening plasmids to be cleared from the population through purifying selection (Vogwill & MacLean, 2015). To avoid extinction, some plasmids can transfer horizontally to lineages with increased fitness, with previous theoretical results establishing sufficient conditions for plasmid maintenance, namely that the rate of horizontal transmission has to be larger than the combined effect of segregational loss and fitness cost (Bergstrom et al., 2000; Stewart & Levin, 1977). Also, some plasmids encode molecular mechanisms that increase their stability in the population, for instance, toxin-antitoxin systems that kill plasmid-free cells (Mochizuki et al., 2006), or active partitioning mechanisms that ensure the symmetric segregation of plasmids upon division (Salje, 2010).

To avoid segregational loss, nonconjugative plasmids lacking active partitioning and postsegregational killing mechanisms tend to be present in many copies per cell, therefore decreasing the probability of producing a plasmid-free cell when randomly segregating plasmids during cell division. But this reduced rate of segregational loss is not sufficient to explain the stable persistence of costly plasmids in the population, suggesting that a necessary condition for plasmids to persist in the population is to carry beneficial genes for their hosts that are selected for in the current environment. However, regimes that positively select for plasmid-encoded genes can be sporadic and highly specific, so plasmid persistence is not guaranteed in the long term. Moreover, even if a plasmid carries useful genes for the host, these can be captured by the chromosome, thus making plasmids redundant and rendering them susceptible to be cleared from the population (Hall et al., 2016). This evolutionary dilemma has been termed the "plasmid paradox" (Harrison et al., 2012).

In this paper, we use a population genetics modeling approach to evaluate the interaction between the number of plasmid copies contained in each cell and the energetic cost associated with carrying each plasmid copy. We consider a nontransmissible, multicopy plasmid (it can only be transmitted vertically) that lacks active partitioning or postsegregational killing mechanisms (plasmids segregate randomly upon division). We will also consider that plasmids encode a gene that increases the probability of survival to an otherwise lethal concentration of an antimicrobial substance, albeit imposing a burden to plasmid-bearing cells in drug-free environments. To estimate parameters of our population genetics model, we used an experimental model system consisting on *Escherichia coli* bearing a multicopy plasmid pBGT (~19 copies per cell) carrying $bla_{\text{TEM-1}}$, a drug resistance gene that produces a β-lactamase that degrades ampicillin and other β-lactam antibiotics (Salverda et al., 2010; San Millan, 2018).

We used computer simulations to evaluate the stability of a multicopy plasmid in terms of the duration and strength of selection in favor of plasmid-encoded genes. This allowed us to numerically estimate the number of copies that maximized plasmid stability under different environmental regimes: drug-free environments, constant exposure to a lethal drug concentration, and intermittent periods of selection. Altogether, our results confirm the existence of two opposing evolutionary forces acting on the number of copies carried by each cell: selection against high-copy plasmids consequence of the fitness cost associated with bearing multiple copies of a costly plasmid and purifying selection resulting from the increased probability of plasmid loss observed in low-copy plasmids.

2 | METHODS

2.1 | Serial dilution protocol

We consider a serial dilution experiment with two types of bacteria: plasmid-bearing (PB) and plasmid-free (PF). Let us denote by n the plasmid copy number (PCN) and argue that this is an important parameter: in the one hand, the selective disadvantage of PB individuals due to the cost of carrying plasmids is assumed to be proportional to n; on the other hand, the PCN determines the heritability of the plasmid.

In our schema, each day starts with a population of N cells that grow exponentially until saturation is reached (i.e., until there are γN cells). At the beginning of the next day, N cells are sampled (at random) and transferred to new media and exponential growth starts again (Figure 1a).

2.2 | Interday dynamics

To model the interday dynamics, we consider a discrete-time model in which the population size is fixed to N. Day i starts with a fraction X_i of PB cells (and $1-X_i$ of PF cells). We consider that

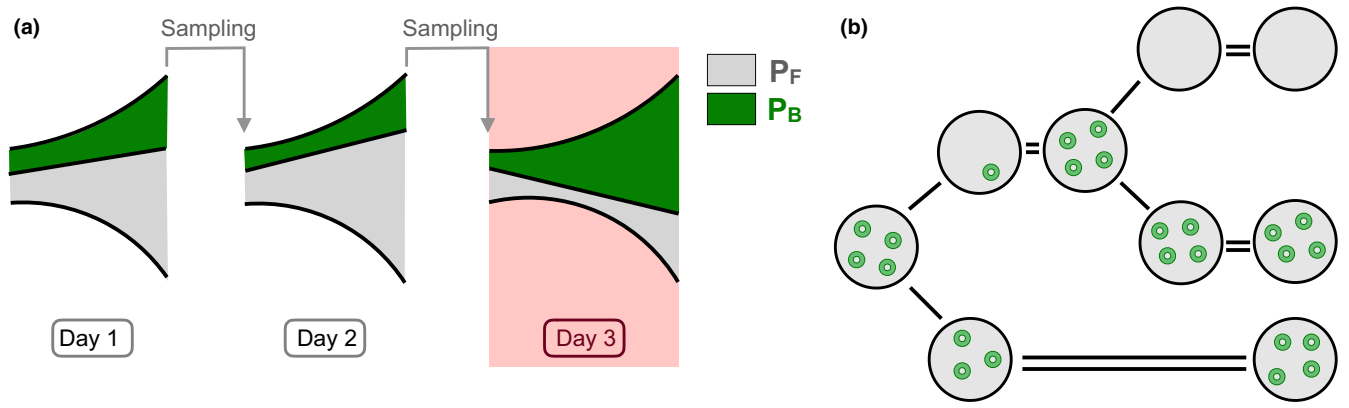

FIGURE 1 Schematic diagram of the model. (a) Serial dilution protocol. PB cells are represented in green, while PF cells are represented in gray. We show 3 days of the experiments. An antibiotic pulse is added during day 3. (b) Segregational loss. Upon cell division, plasmids are segregated at random between the two daughter cells. Then, the plasmids are replicated until the PCN is 4. When a cell inherits no plasmid, it becomes plasmid-free.

the fitness cost associated with plasmid maintenance; κ_n is proportional to the PCN, that is, $\kappa_n = \kappa n$. This means that, at the end of day i, the number of PF cells is proportional to their initial frequency $1-X_i$, while the number of PB cells is proportional to their initial frequency X_i multiplied by $(1-\kappa_n)<1$. So, at the end of day i, the fraction of PB cells would be

$$\frac{(1-\kappa_n)X_i}{(1-\kappa_n)X_i+1-X_i}.$$

In addition, PB cells can lose their plasmids and become PF and with probability μ_n, so, at the end of day i, the fraction of PB cells needs to be multiplied by $(1-\mu_n)$.

At the beginning of day $i+1$, we sample N individuals at random from the previous generation. Since N is very large, we can neglect stochasticity and assume that the fraction of PB cells at the beginning of day $i+1$ is equal to their fraction at the end of day i, that is,

$$X_{i+1} = f(X_i) := \frac{(1-\kappa_n)X_i}{(1-\kappa_n)X_i+1-X_i}(1-\mu_n), \quad i \geq 1. \tag{1}$$

Additionally, we aim to modeling selection for plasmid-encoded genes. For plasmids carrying antibiotic resistance genes, this is achieved by exposing the population to antibiotic pulses. Individuals with no plasmids suffer more from this treatment, so, at each pulse, we observe an increment in the relative frequency of the PB subpopulation. To model this phenomenon, we assume that, in the presence of antibiotic, PF individuals exhibit a selective disadvantage represented by parameter $\alpha \in [0,1]$.

For instance, if an antibiotic pulse occurs at day i, all PB cells survive, (there are NX_i), but the PF cells die with probability α, so only $N(1-\alpha)(1-X_i)$ survive. So, the fraction of PB individuals, right after the antibiotic pulse becomes

$$g(X_i) := \frac{X_i}{X_i+(1-\alpha)(1-X_i)}.$$

Then, cells grow exponentially again, as in a normal day, so that, at the end of the day, the fraction of PB cells is $f(g[X_i])$.

If we consider that the pulses occur at generations T, $2T$,..., the frequency process becomes

$$X_{i+1} = \begin{cases} f(g(X_i)) = \dfrac{(1-\kappa_n)X_i}{1-\alpha+(\alpha-\kappa_n)X_i}(1-\mu_n) & \text{if } i=jT,\ j=1,2\ldots \\ f(X_i) = \dfrac{(1-\kappa_n)X_i}{(1-\kappa_n)X_i+1-X_i}(1-\mu_n) & \text{otherwise.} \end{cases} \tag{2}$$

2.3 | Intraday dynamics

For the intraday dynamics, day i starts with a population of N cells ($N \sim 10^5$ in the experiment) that grow exponentially until saturation is reached (i.e., until there are γN cells). The initial fraction of PB cells is X_i. We assume that, in the absence of antibiotic, the population evolves as a continuous time multitype branching process $\mathbf{Z}_t = (Z_t^0, Z_t^1)$, where Z_t^0 (resp Z_t^1) is the number of PB cells (resp. PF cells). The reproduction rate (or *Malthusian fitness*) of PB (resp. PF) individuals is r (resp. $r+\rho_n$), with $\rho_n > 0$ (since PB individuals have some disadvantage due to the cost of plasmid maintenance). Following (González Casanova et al., 2016), we assume that $\rho_n \sim N^{-b}$ for some $b \in (0,1/2)$ (this regime is known as *moderate-strong selection*).

We consider plasmids that lack active partitioning systems (Salje, 2010), so, at the moment of cell division, each plasmid randomly segregates into one of the two new cells. Once in the new host, the plasmids replicate until reaching n copies. If, however, one of the two new cells has all the n copies, the other one will not carry any plasmid copy and becomes PF. Thus, we make the simplifying assumption that the daughter of a PB cell becomes PF with probability 2^{-n} (segregational loss rate), as illustrated in Figure 1b. Therefore, at every branching event, an individual splits in two. Plasmid-free individuals only split in two PF individuals. Plasmid-bearing individuals can split in one PF individual and one

PB individual with probability 2^{-n} (if all the plasmids go to one of them) or they can split in two plasmid-bearing individuals with probability $1-2^{-n}$.

Let $M(t) = \{M_{i,j}(t): i,j = 0,1\}$ be the mean matrix given by $M_{i,j}(t) = \mathbb{E}_{\mathbf{e}_i}\left(Z_t^j\right)$, the average size of the type j population at time t if we start with a type i individual. According to (Athreya & Ney, 2004; section V.7.2), $M(t)$ can be calculated as an exponential matrix

$$M(t) = e^{tA} \quad \text{where} \quad A = \begin{pmatrix} r+\rho_n & 0 \\ r2^{-n} & r\left(1-2^{-n}\right) \end{pmatrix}.$$

More precisely,

$$M(t) = \begin{pmatrix} e^{(r+\rho_n)t} & 0 \\ \dfrac{r2^{-n}}{r2^{-n}+\rho_n}\left(e^{(r+\rho_n)t} - e^{r(1-2^{-n})t}\right) & e^{r(1-2^{-n})t} \end{pmatrix}.$$

Let σ be the duration of the growth phase. Since N is very large, one can assume that reproduction is stopped when the expectation of the number of descendants reaches γN, that is, that σ satisfies

$$\begin{aligned}\gamma N &= (1-X_i)N\left(M_{0,0}(\sigma)+M_{0,1}(\sigma)\right)+xN\left(M_{1,0}(\sigma)+M_{1,1}(\sigma)\right)\\ &= Ne^{r\sigma}\left(e^{\rho_n\sigma}+\rho_n X_i\,\frac{e^{-r2^{-n}\sigma}-e^{\rho_n\sigma}}{r2^{-n}+\rho_n}\right).\end{aligned}$$

Since $\rho_n \sim N^{-b}$, we have for large enough N that

$$\sigma \simeq \frac{\log\gamma}{r}.$$

Since $\gamma N >> 1$, we can assume that the number of PB (resp. PF) cells at the end of the day is equal to its expected value. Therefore, the fraction of PB cells at the end of day i is equal to

$$\frac{X_i M_{1,1}(\sigma)}{(1-X_i)\left(M_{0,0}(\sigma)+M_{0,1}(\sigma)\right)+X_i\left(M_{1,0}(\sigma)+M_{1,1}(\sigma)\right)} = \frac{X_i e^{-(r2^{-n}+\rho_n)\sigma}}{(1-X_i)+X_i\frac{r2^{-n}+\rho_n e^{-(r2^{-n}+\rho_n)\sigma}}{r2^{-n}+\rho_n}}. \tag{3}$$

This corresponds to Equation (2) with parameters

$$\kappa_n = \frac{\rho_n\left(1-e^{-(r2^{-n}+\rho_n)\sigma}\right)}{r2^{-n}+\rho_n} \sim \sigma\rho_n = \sigma\rho n \quad \text{and} \quad \mu_n = 1-\frac{r2^{-n}+\rho_n}{r2^{-n}e^{(r2^{-n}+\rho_n)\sigma}+\rho_n} \sim_{n\to\infty} r\sigma 2^{-n}. \tag{4}$$

The importance of these formulas is that they connect measurable quantities with theoretical parameters, leading to a method to estimate the parameters of the model from experiments, which is the spirit of the experiment described in the following section.

2.4 | Model parametrization

Our goal is to use the interday model to evaluate the long-term dynamics of plasmid-bearing populations in terms of the cost associated with carrying plasmids and the fitness advantage conferred by the plasmid in the presence of positive selection. To quantify these parameters experimentally, our approach consisted in two phases: (1) from growth kinetic experiments, we estimate parameters ρ, r, and σ of the interday model, and (2) we perform competition experiments in a range of drug concentrations to obtain μ_n and κ_n using Equation (4) of the intraday model.

Our experimental model system consisted in *E. coli* K12 carrying pBGT, a nontransmissible multicopy plasmid used previously to study plasmid dynamics and drug resistance evolution (Hernandez-Beltran

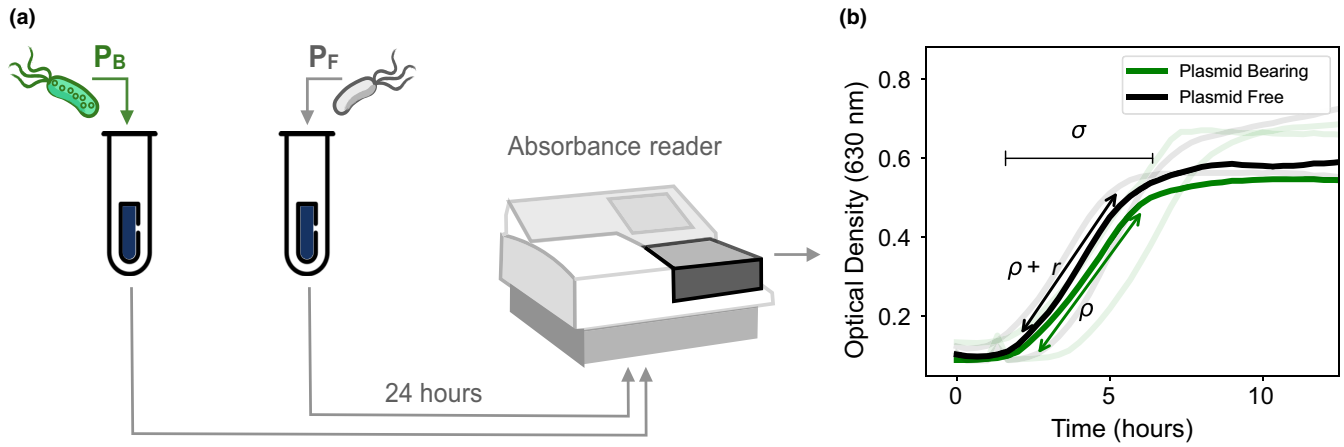

FIGURE 2 Growth kinetic experiment. (a) Schematic diagram illustrating a bacterial growth experiment performed in drug-free media separately for PB and PF populations. We used an absorbance microplate reader to measure the optical density (OD_{630}) at different timepoints during the 24-h experiment. (b) Growth curves of PB (green) and PF (black) strains, with replicate experiments represented as shaded curves. The duration of the exponential phase, σ, was estimated by identifying the start of exponential phase and the time elapsed before reaching carrying capacity. Parameter ρ refers to the maximum growth rate of the PB population, while the selective advantage of the PF strain is represented with r.

et al., 2020, 2022; Rodriguez-Beltran et al., 2018; San Millan et al., 2016). Briefly, pBGT is a ColE1-like plasmid with ~19 plasmid copies per cell, lacking the necessary machinery to perform conjugation or to ensure symmetric segregation of plasmids upon division. This plasmid carries a GFP reporter under an arabinose-inducible promoter and the bla_{TEM-1} gene that encodes for a β-lactamase that efficiently degrades β-lactam antibiotics, particularly ampicillin (AMP). The minimum inhibitory concentration (MIC) of PB cells to AMP is 8192 mg/L, while the PF strain has a MIC of 4 mg/L (see Appendix A).

Growth experiments were performed in 96-well plates with lysogeny broth (LB) rich media and under controlled environmental conditions. Using a plate absorbance spectrophotometer, we obtained bacterial growth curves that enabled us to estimate the maximal growth rate of the PB and PF strains, corresponding to r and ρ_n in the intraday model (Hall et al., 2014; Figure 2a and Appendix C). As expected, we observed a reduction in bacterial fitness of the PB subpopulation, expressed in terms of a decrease in its maximum growth rate when grown in isolation. The metabolic burden associated with carrying the pBGT plasmid ($n = 19$) was estimated at 0.108 ± 0.067 (Figure 2b).

We then performed a 1-day competition experiment consisting of mixing PB and PF subpopulations with a range of relative abundances and exposing the mixed populations to environments with increasing drug concentrations (see Figure 3a for a schematic of the experimental protocol). Previous studies have used a similar approach to determine a selection coefficient (Dykhuizen, 1990), a quantity that was used to show that selection of resistance can occur even at sublethal antibiotic concentrations (Gullberg et al., 2011).

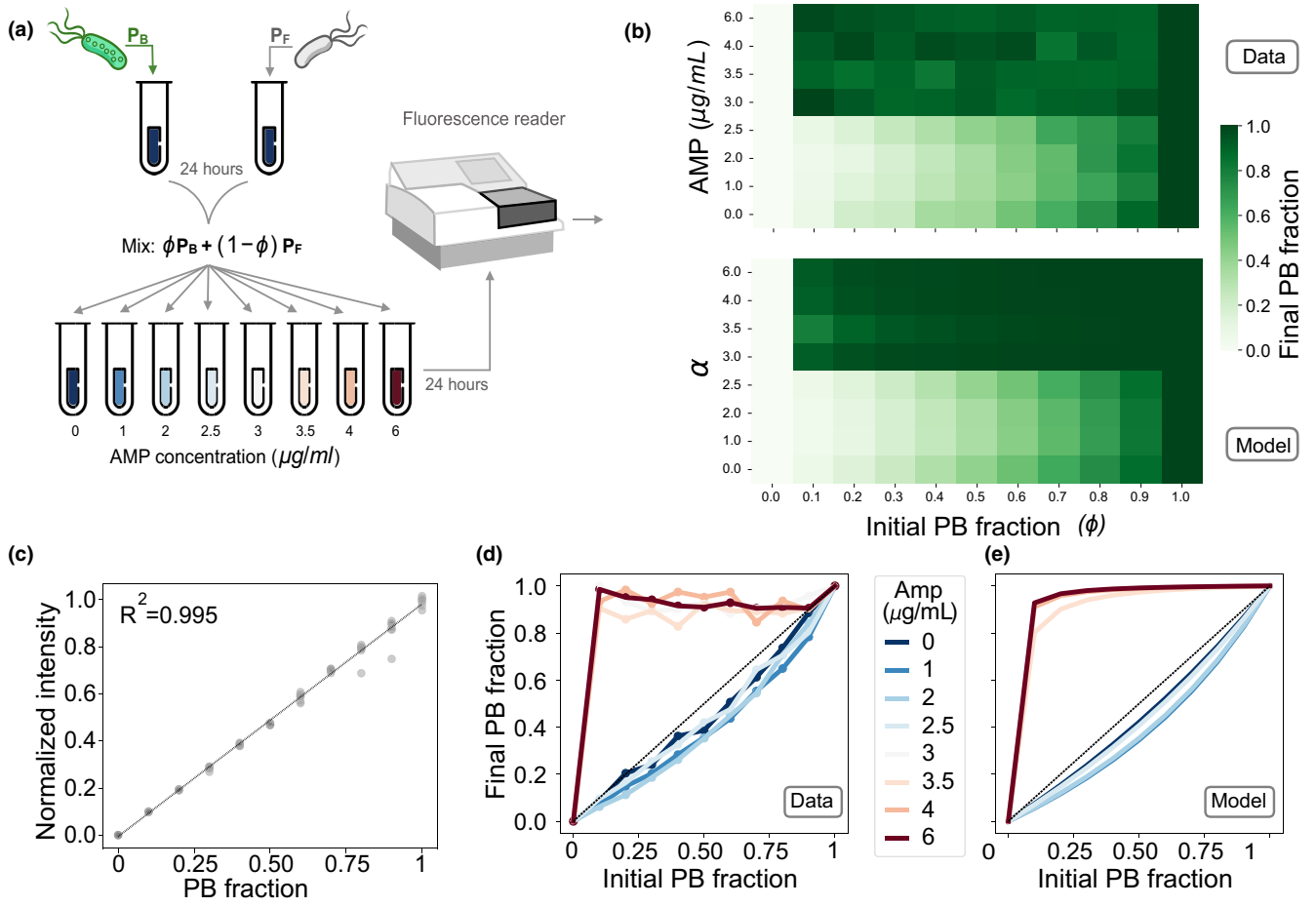

FIGURE 3 Competition experiment under a range of drug concentrations. (a) Schematic diagram illustrating an experiment where PB and PF are mixed at different relative abundances and submitted to a range of ampicillin concentrations (0, 1, 2, 2.5, 3, 3.5, 4, and 6 μg/ml). We use a fluorescence spectrophotometer to estimate the relative abundance of plasmid-bearing cells in the population after 24 h of growth. (b) Final PF frequency (illustrated in a gradient of green) for different initial fraction of PB cells and selection coefficients (top: Data; bottom: Model). (c) Control experiment illustrating that normalized fluorescence intensity is correlated with the fraction of the population carrying plasmids. Each dot presents a replica and the dotted line a linear regression ($R^2 = .995$). (d) Experimental iterative map showing the existence of a minimum drug concentration that rescues the PB population (red lines). At low drug concentrations (blue lines), the PB population decreases in frequency. (e) Theoretical iterative map obtained by numerically solving Equation (2) for a range of strength of selections and initial PB frequencies. By fixing κ_n (previously estimated by growing each strain in monoculture), we fitted parameter α in Equation (2) to the experimental data. Colors indicate the strength of selection (in blue), values of α where the cost of carrying plasmids is stronger than the benefit resulting from positive selection, yielding curves below the identity line. Red curves represent simulations obtained with values of α strong enough to kill PF cells, thus increasing PB frequency in the population.

TABLE 1 Model parameters estimated using growth curves experiments in the absence of antibiotics

Parameter	Measured value	Formula	Estimated value	Description
r	0.435435	NA	NA	Plasmid strain growth rate
ρ	0.052334	NA	NA	WT growth rate advantage
σ	6.074089	NA	NA	Exponential phase duration
μ_n	NA	$\mu_n = 1 - \frac{r2^{-n}+\rho}{r2^{-n}e^{(r2^{-n}+\rho)\sigma}+\rho}$	5.938e−06	1-day fraction of segregants
κ_n	NA	$\kappa_n = \frac{\rho\left(1-e^{-(r2^{-n}+\rho)\sigma}\right)}{r2^{-n}+\rho}$	0.272313	Fitness cost
n	19	NA	NA	Plasmid copy number

TABLE 2 Model parameter estimated by fitting Equation (4) to experimental data obtained for a range of ampicillin concentrations

Amp	κ_n	α
0.0	0.272276	0.0
1.0	0.272276	−0.37781
2.0	0.272276	−0.332662
2.5	0.272276	−0.058457
3.0	0.272276	0.992911
3.5	0.272276	0.9801
4.0	0.272276	0.992075
6.0	0.272276	0.99373

Figure 3b shows the final PF frequency obtained for different initial population structures and strengths of selection.

The fitness cost associated with carrying plasmids in our inter-day model was estimated from the proportion of PB cells at the end of a competition experiment. This quantity can be obtained from the normalized fluorescent intensity of the bacterial culture, measured with a fluorescent spectrophotometer or with flow cytometry (Figure 3c shows a linear relationship between both quantities). Figure 3d shows the end-point bacterial density resulting from competition experiments with different initial fractions of PB cells exposed to a range of AMP concentrations. Note that, at low AMP concentrations (blue lines), the frequency of plasmid bearing is below the identity, consistent with plasmids imposing a fitness cost to PB cells. By contrast, at high AMP concentrations (red lines), plasmid-free cells are killed and the population is almost exclusively conformed by PB cells.

In the model, since PCN is a fixed parameter, the PB fraction resulting from a competition experiment in the absence of selection only depends on the cost associated with plasmid bearing. Therefore, by fitting Equation (1), we estimated that the cost associated with carrying $n = 19$ copies of pBGT was $\kappa_n = 0.272$. Furthermore, by fixing this parameter and incorporating antibiotics, we estimated the selective pressure α for different antibiotic concentrations by fitting Equation (2) to the experimental data. Figure 3e illustrates that at low antibiotic concentrations (small values of α) the frequency of the population is low, while higher values of α result in an increased PB frequency. Table 1 summarizes parameter values estimated for each strain in our model, and Table 2 shows the correspondence between antibiotic concentrations and α.

3 | RESULTS

3.1 | Segregational instability in the absence of selection

Our first aim was to evaluate the stability of a costly multicopy plasmid in the absence of selection for plasmid-encoded genes (i.e., without antibiotics). By numerically solving Equation (1), we evaluated the stability of the PB subpopulation in terms of the mean PCN and the fitness cost associated with carrying each plasmid copy (see Appendix C). As expected, in the absence of selection, plasmids are always cleared from the population with a decay rate that depends on PCN. We define the time-to-extinction as the time when the fraction of PB cells goes below an arbitrary threshold.

For cost-free plasmids (i.e., when $\kappa = 0$), the time-to-extinction appears to be correlated to PCN (Figure 4a). By contrast, if we consider a costly plasmid ($\kappa > 0$) and that the total fitness cost is proportional to the PCN (i.e., if PCN = n, the total cost is $\kappa_n = \kappa n$), then extinction occurs in a much faster timescale (Figure 4b—notice the difference of timescales with Figure 4a). As shown in Figure 4b, small PCN values are associated with a high probability of segregational loss, and therefore the time-to-extinction increases with PCN. However, large values of PCN are associated with higher levels of instability due to the detrimental effect on host fitness resulting from carrying multiple copies of a costly plasmid.

This observation indicates the existence of a nonlinear relationship between the stability of plasmids and the mean PCN of the population. To further explore this association, we computationally estimated the time-to-extinction in a long-term setting (simulations running up to 500 days) for different values of PCN and fitness cost. As expected, Figure 4c shows an accelerated rate of plasmid loss in costly plasmids. Crucially, there appears to be a critical PCN that maximizes the time-to-extinction, which depends on the per-cell plasmid cost. The time-to-extinction gives a notion of the stability of plasmids, but this measure may not apply if we introduce antibiotics and therefore avoid plasmid extinction. For this reason, we also quantified plasmid stability by measuring the area under the curve (AUC) of simulation trajectories similar to those in Figure 4b. The heatmap illustrated in Figure 4d shows this measure highlighting the existence of a region in the cost-PCN plane, at intermediary PCN values, where plasmid stability is maximized.

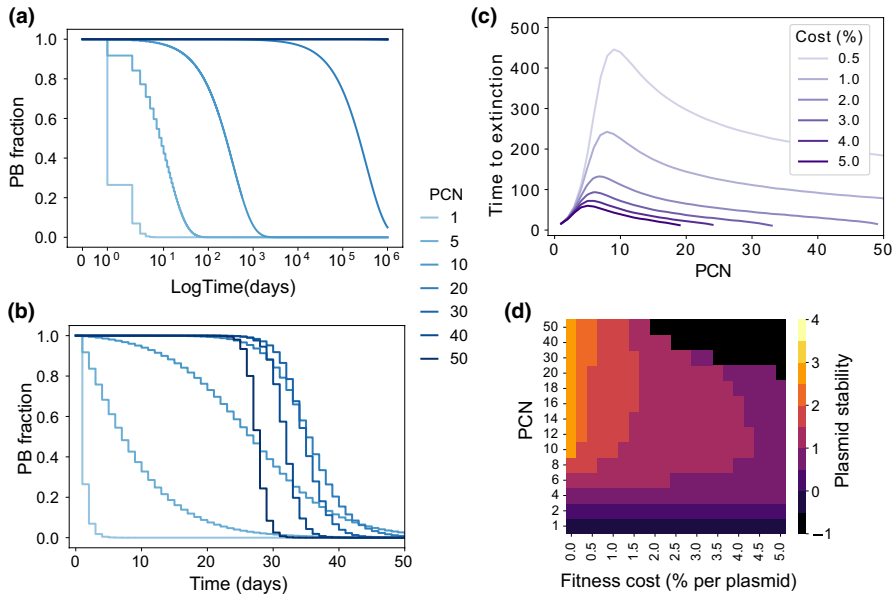

FIGURE 4 Numerical results for the model without selection for plasmid-encoded genes. (a) Plasmid frequency as a function of time for a cost-free plasmid ($\kappa = 0$). Note how, as the PCN increases, the stability of plasmids also increases, although eventually all plasmids will be cleared from the system. (b) Dynamics of plasmid loss for strains bearing a costly plasmid ($\kappa = 0.0143$). In this case, low-copy plasmids (light blue lines) are highly unstable, but so are high-copy plasmids (dark blue lines). (c) Time elapsed before plasmid extinction for a range of PCNs. A very costly plasmid ($\kappa = 5\%$) is represented in dark purple, while the light purple line denotes a less costly plasmid ($\kappa = 0.5\%$). (d) Plasmid stability for a range of fitness costs and PCNs (discrete colormap indicates level of stability, yellow denotes higher stability, while dark purple denotes rapid extinction). Stability is measured as the area under the curve (AUC) of trajectories similar to those in (b), expressed in $\log_{10}$ scale. Notice that, for intermediate fitness costs, the PCN that maximizes plasmid stability can be found at intermediate values.

3.2 | Evaluating the role of selection in the stability of plasmids

To study the interaction between plasmid stability and the strength of selection in favor of PB cells, we assumed that the plasmid carries a gene that confers a selective advantage to the host in specific environments (e.g., resistance to heavy metals or antibiotics). For the purpose of this study, we will consider a bactericidal antibiotic (e.g., ampicillin) that kills PF cells with a probability that depends on the antibiotic dose. This results in a competitive advantage of the PB cells with respect to the PF subpopulation in this environment. We denote the intensity of this selective pressure by α.

Figure 5a–g illustrates plasmid dynamics over time for different values of α, obtained numerically by solving Equation (2) with a fixed PCN ($n = 19$) and drug always present in the environment ($T = 1$). In our model, then we found a critical dose that stabilizes plasmids in the population, that is, the minimum selective α, $MS\alpha = \kappa_n + \mu_n(1 - \kappa_n)$; see Appendix B). The existence of a minimum selective concentration (MSC) that maintains plasmids in the population is a feature used routinely by bioengineers to stabilize plasmid vectors through selective media (Kumar et al., 1991). Recall that in our model the PF MIC is $\alpha = 1$; therefore, the $MS\alpha$ can be directly compared with the MSC/MIC ratio previously proposed (Greenfield et al., 2018; Gullberg et al., 2011) as a concern factor on the selection of resistant strains in the environment.

As illustrated in Figure 5h, both low-copy and high-copy plasmids are inherently unstable and therefore the selective pressure necessary to stabilize them is relatively high, particularly for costly plasmids. Interestingly, at intermediate PCN values, the selective conditions necessary to stabilize plasmids are considerably less stringent than for low- and high-copy plasmids. This is the result of the nonlinear relationship between MSα and n; since μ_n decreases exponentially with n, κ_n increases only linearly with n.

Figure 5i shows the time elapsed before converging to a steady state (either extinction or persistence) for different values of α and PCN. As α increases, the cost of plasmid bearing is compensated by the benefit of carrying the plasmid and therefore plasmids are maintained in the population for longer. Note that at large values of α, plasmid-free cells are killed immediately independently of the mean PCN of the population, resulting very fast in a population composed almost exclusively of plasmid-bearing cells. Note that, in the case, the steady state $x^* = 1 - \mu_n \frac{1-\kappa_n}{\alpha-\kappa_n}$ is achieved independently of the initial fraction of PB cells (see Appendix B), which is consistent with previous results (Yurtsev et al., 2013).

3.3 | Plasmid stability in periodic environments

The purpose of this section is to understand the ecological dynamics of the plasmid-bearing population in fluctuating environments, that is, when periodic antibiotic pulses are administered. We started by

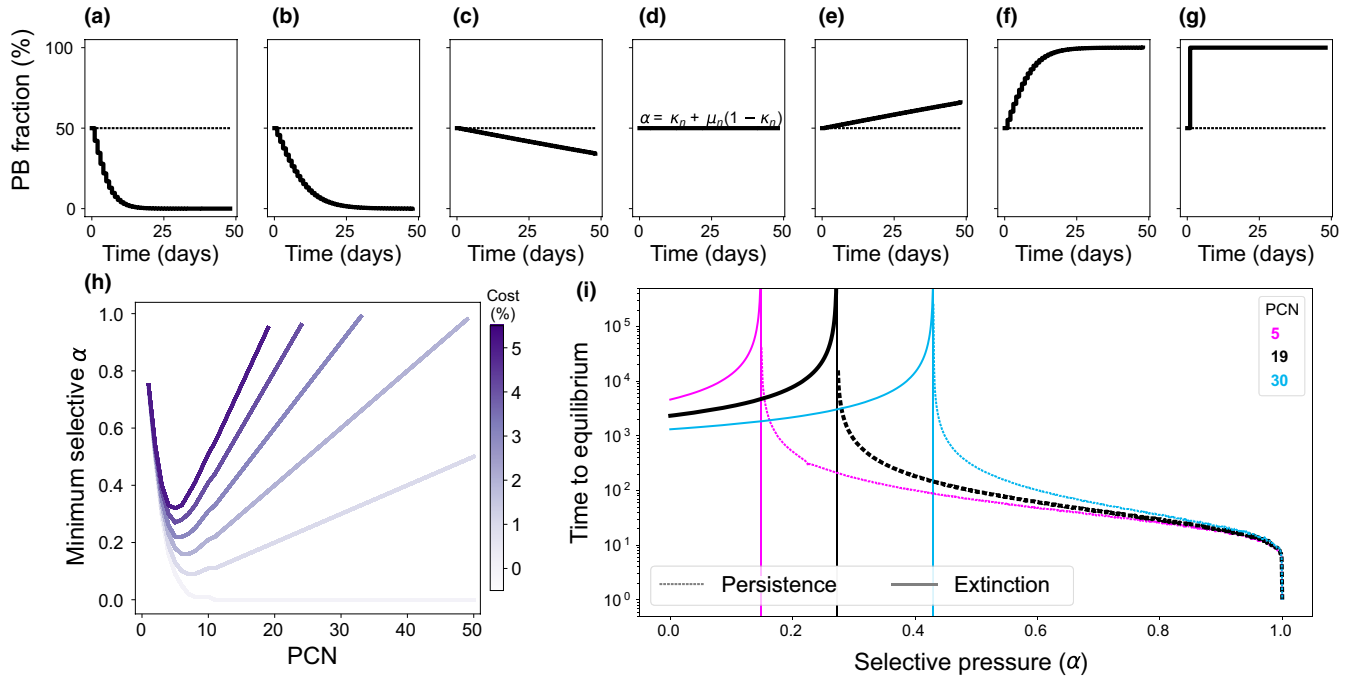

FIGURE 5 Numerical results illustrating the effect of a constant selective pressure in the stability of nontransmissible multicopy plasmids. (a–g) Each box illustrates the temporal dynamics of the plasmid-bearing subpopulation in a pairwise competition experiment inoculated with equal initial fractions of *PF* and *PB*. From left to right, $\alpha = 0$, 0.2, 0.26, 0.28, 0.6, and 1. The dotted line denotes $MS\alpha = \kappa_n + \mu_n(1-\kappa_n)$ for $n = 19$ and $\kappa_n = 0.27$. Note that for values of $\alpha < MS\alpha$, plasmids are unstable and eventually cleared from the population, while for $\alpha > MS\alpha$ the plasmid-bearing subpopulation increases in frequency until reaching fixation. For $\alpha = MS\alpha$, the selective pressure in favor of the plasmid compensates its fitness cost and therefore the plasmid fraction remains constant throughout the experiment. (h) Minimum selective pressure required to avoid plasmid loss for a range of PCNs. Different curves represent plasmids with different fitness costs (light purple denotes cost-free plasmids and dark purple a very costly plasmid). Note that, for costly plasmids, there exists a nonmonotone relationship between $MS\alpha$ and PCN. (i) Time elapsed before plasmid fraction in the population is stabilized, for different copy numbers (5 in magenta, 19 in black, and 30 in cyan). Dotted lines represent plasmid fixation, while dashed lines denote stable coexistence between plasmid-free and plasmid-bearing subpopulations, and solid lines plasmid extinction. The vertical line indicates $MS\alpha$, the minimum selective pressure that stably maintains plasmids in the population. Black letters indicate the parameter values used in the examples shown in (a–g).

exploring the time duration a PB population can survive without antibiotics before being rescued by a strong antibiotic pulse (Figure 6a). Consistently with the results from the first section, lower plasmid costs result in increased rescue times, suggesting that a lesser rate of antibiotic exposure is required for their maintenance. In Figure 6b, we quantified this minimal period as a function of PCN and α. Note that higher values of α correspond to longer periods, which follows from the fact that a higher selective pressure increases the PB frequency. Figure 6d illustrates this critical period for PCN = 19.

In periodic environments, the relative abundance of the PB population is driven to zero (extinction) or reaches a steady state in which the plasmid fraction oscillates around an equilibrium frequency (persistence). In Figure 6c, times to stabilization were estimated for the strong selection regime ($\alpha = 0.99$), using the same PCNs as in Figure 5i. Notice that the time-to-extinction is larger than the time to reach the periodic attractor. In both cases, the maximal time to rescue and the minimum period to avoid loss, we observe a nonmonotone effect of PCN and, therefore, a range of PCNs whereby plasmid stability is maximized. This is consistent with what we observed without antibiotics (Figure 4c) and with constant environments (Figure 5h).

3.4 | Optimal PCN depends on the rate of environmental fluctuation

In this section, we aim at exploring the concept of optimal PCN and how it depends on the environment. To do so, we define the optimal PCN (hereafter denoted PCN*) as the PCN that maximizes the area under the curve (AUC) of the PB frequency over time. This notion of stability was already introduced in Figure 4d and has the advantage that it can be used when the PB fraction goes to 0, to a fixed equilibrium, or when it oscillates.

First, we calculated PCN* for a range of plasmid fitness costs in the absence of selection (black solid line of Figure 7a) and found that PCN* is inversely correlated with the plasmid fitness cost. In order to compare the optimal PCN predicted by the model with PCN values found in other experimental plasmid-host associations, we searched the literature for studies that measure both PCN and fitness cost. These values are summarized in Table 3 and illustrated in Figure 7a. The values of PCN found in the literature were below the predicted PCN* in an antibiotic-free regime (black solid line), suggesting that plasmids would be unstable in the absence of selection. But, crucially, PCN values obtained from the literature are within the

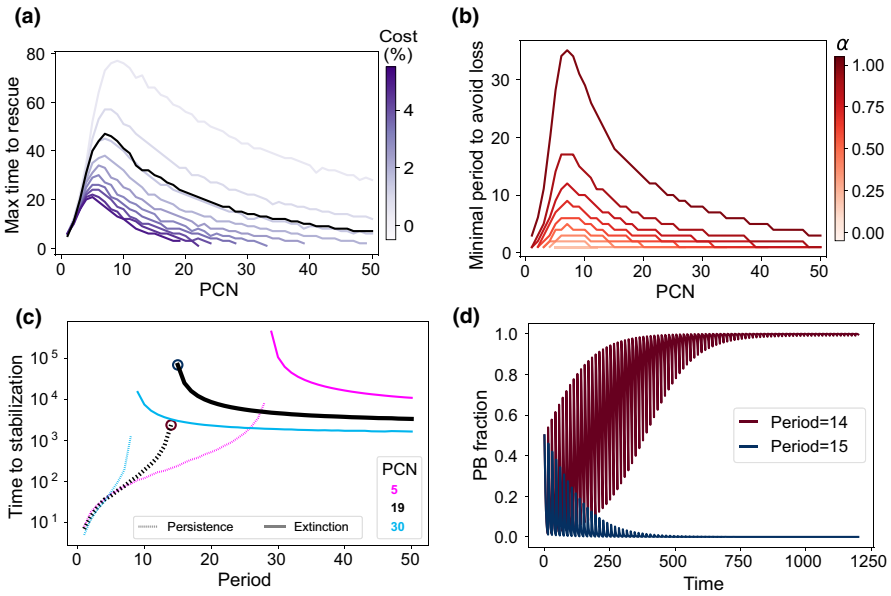

FIGURE 6 Numerical results of the model in periodic environments. (a) Maximum time a plasmid population can grow without antibiotics to avoid plasmid loss when applying a strong antibiotic pulse. Curves represent how this time is affected by PCN. Blue intensity represents plasmid cost, and black line indicates results using the pBGT parameters. (b) Minimal period required to avoid plasmid extinction. Simulations were performed using the pBGT measured cost ($\kappa = 0.014$). Red intensity represents different values of α. Note that higher values of α increase the minimal period. (c) Time required for trajectories to stabilize for copy numbers 5, 19, and 30 using $\alpha = 0.99$ and the measured cost per plasmid. Note that there is a critical period that defines fixation or coexistence marked by red and blue circles on the PCN = 19 (black) curve. (d) Trajectories for the critical periods of PCN = 19 starting from 0.5 PB-PF frequency. Note that 1-day period difference leads to opposite outcomes.

blue-shaded area that represents the PCN* estimated for different environments (observe the nonlinear relationship between α, PCN*, and cost, in line with our previous findings).

These observations would be consistent with the constant use of antibiotics at low doses that reduces the optimal PCN. However, similar PCN* values can be achieved by administering higher doses of antibiotics periodically, as illustrated in Figure 7b for the case of pBGT. Notice again the nonlinear relationship between PCN* and the frequency of antibiotic exposure. At very low frequencies, the PB population goes extinct before the first antibiotic pulse and intermediate PCNs maximize the AUC as in Figure 4d. At high antibiotic frequencies, the PB population persists and oscillates around some value that increases with PCN. This is consistent with a previous experimental study that evaluated the stability of costly plasmids in terms of the frequency of environmental fluctuation (Stevenson et al., 2018).

Periodic environments provided us with insights into how selection acts on the mean PCN of the population, but natural environments are not periodic but randomly alternate between intervals of positive and negative selection. The role of environmental stochasticity in the stability of multicopy plasmids (Münch et al., 2019; Rodriguez-Beltran et al., 2018) and, in general, in the population dynamics of asexual populations has been widely studied (Kussell & Leibler, 2005; Raj & van Oudenaarden, 2008). In our model, we generated stochastic environments that randomly switch from antibiotic-free to antibiotic for a period of 1000 days. Each random environment is represented by a sequence of 1s and 0s, corresponding to days with and without antibiotics, respectively. Therefore, stochastic environments can be characterized by their Shannon's entropy (environmental entropy, H) and the fraction of days with drug exposure (antibiotic rate, AR) (see Appendix C). Environments were classified into "High" and "Low" depending on whether the AR was greater or lower than 0.5. Mind that each value of H corresponds to two AR values AR and 1 − AR.

Panels on Figure 7d,e show the PCN* found by applying the stochastic environments ordered by entropy (or by AR), for different values of α. For low values of α, only high antibiotic rates lead to plasmid persistence. Notice the nonlinear relationship between PCN* and AR, similar to the observed for the period in the deterministic setting; PCN* decreases with AR at low values (corresponding to extinction) but increases with AR at high values (corresponding to persistence). For higher values of α, we observed that high AR always leads to persistence, while low AR can lead to extinction if entropy is low. In fact, these low values of the entropy corresponded to long periods without antibiotics that drove the PB population to extinction. Another interesting remark is that the distribution of obtained PCN*s is multimodal; at fixed entropy, plasmid persistence is achieved by high values of AR that correspond to high PCN* or by low values of AR that correspond to a small value of PCN*. Similarly, a fixed value of α corresponds to two values of PCN* depending on the antibiotic rate (Figure 7c).

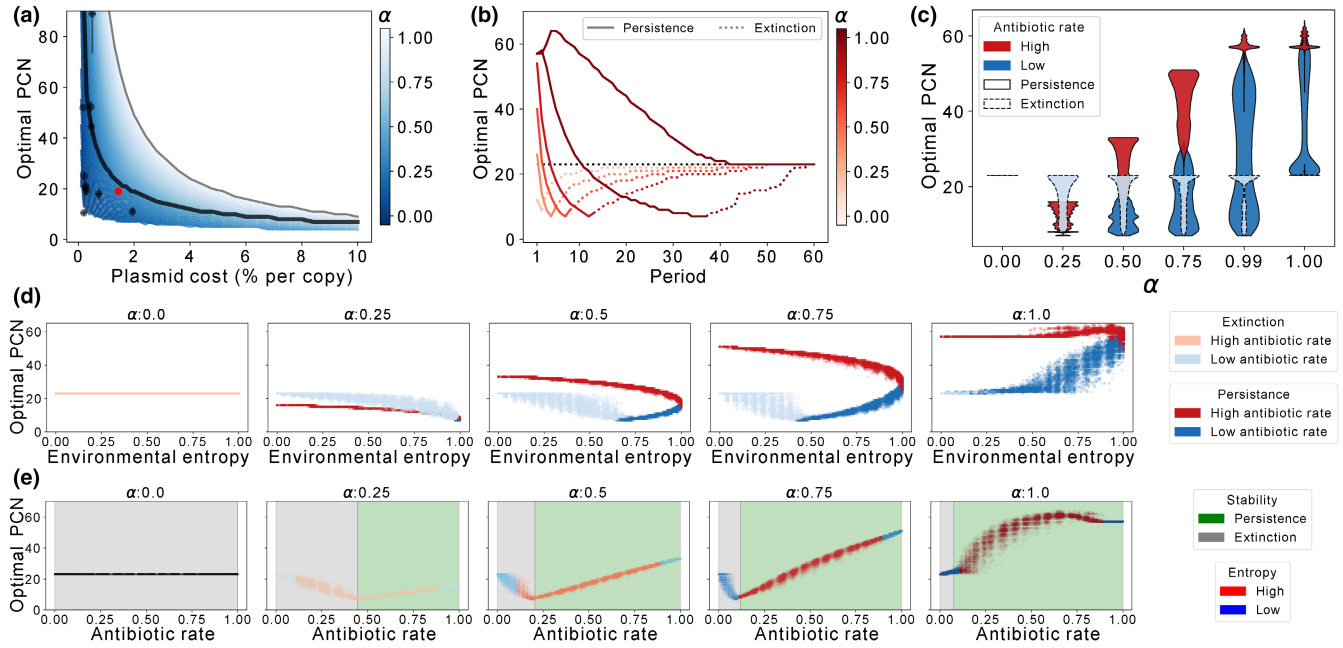

FIGURE 7 Optimal PCNs in fluctuating environments. (a) Optimal plasmid copy number (PCN*) as the number of copies that maximizes the area under the curve of Figure 4b. PCN* decreases exponentially as we increase the fitness cost associated with carrying plasmids, as indicated in black solid line. Black dots show some PCN-costs data obtained from the literature. Red dots indicate the values of pBGT. Blue-scale lines indicate optimal PCN curves for many values of α. Light-blues indicate higher values of α whereas dark-blues indicate lower values of α. Gray line shows the max PCN for the corresponding plasmid cost. (b) Optimal PCN in periodic environments. Each curve corresponds to a value of α. Black line shows $\alpha = 0$. Observe that for very short periods optimal PCNs are high, then for certain period the optimal PCN reaches a minimum then as period increases, the optimal PCN tends to the optimal of $\alpha = 0$. (c–e) Optimal PCNs using random environments. (c) Environments are classified by their rate of days with antibiotics, the rate differences produce a multimodal outcome, where higher rates increase the optimal PCN and vice versa. Simulations using the same environments were made for different αs. Note that α intensity increases the separation of the modes. Modes are also classified by their stability, persistence marked with a solid border line and extinction with a dashed border line. (d) Panel of optimal PCNs plotted by the environment entropy for sample α. Environments are classified by their antibiotic rate. (e) Panel of optimal PCNs plotted by the environment antibiotic rate for sample α. Environments are classified by their entropy.

4 | DISCUSSION

In this work, we used a population genetics modeling approach to study how nontransmissible plasmids are maintained in bacterial populations exposed to different selection regimes. In particular, we considered a small multicopy plasmid that lacks an active partitioning mechanism and therefore segregates randomly upon cell division. Multicopy plasmids are prevalent in clinical bacteria and usually carry antimicrobial resistance genes that can be transferred between neighboring bacterial cells (Ares-Arroyo et al., 2022), as well as other evolutionary benefits that go well beyond horizontal transfer (Rodríguez-Beltrán et al., 2021). For instance, as multicopy plasmids are present in numerous copies per cell, the mutational supply increases proportionately and, once a beneficial mutation appears, its frequency can be amplified during plasmid replication. This results in an accelerated rate of adaptation to adverse environmental conditions (San Millan, 2018) and enables evolutionary rescue (Santer & Uecker, 2020). Also, multicopy plasmids increase the genetic diversity of the population, thus enhancing survival in fluctuating environments (Hernandez-Beltran et al., 2022) and allowing bacterial populations to circumvent evolutionary trade-offs (Rodriguez-Beltran et al., 2018).

While the benefits of carrying plasmids may be clear under certain circumstances, their maintenance can be associated with a considerable energetic cost in the absence of selection for plasmid-encoded genes. This trade-off between segregational stability and fitness cost has been shown to drive ecological and evolutionary dynamics in plasmid-bearing populations (Paulsson & Ehrenberg, 1998), resulting from multilevel selection acting on extra-chromosomal genetic elements (Garoña et al., 2021; Paulsson, 2002). Plasmid population dynamics resulting from random segregation and replication result in a complex interaction between plasmid copy number, genetic dominance, and segregational drift, with important consequences in the fixation probability of beneficial mutations (Ilhan et al., 2019) and the repertoire of genes that can be carried in mobile genetic elements (Rodriguez-Beltran et al., 2019). Besides a reduction in segregational instability, increasing the number of plasmids each cell carries also results in an increase in gene dosage (Dimitriu et al., 2021; Million-Weaver et al., 2012) and expression variability of plasmid-encoded genes (Hernandez-Beltran et al., 2022; Jahn et al., 2016). For this reason, plasmid control in wild-type bacteria is a tightly regulated process (Del Solar & Espinosa, 2000) that depends on the environment and the host's genetics (Alonso-del Valle et al., 2021). Precise

TABLE 3 Plasmid copy number and plasmid costs from literature

Name	Plasmid type	Species	PCN	PCN SD	Cost	Cost SD	References
pB1006	ColE1	*Haemophilus influenzae* RdKW20	10.530	1.112	0.021	0.012	Santos-Lopez et al. (2017)
pB1005	ColE1	*Haemophilus influenzae* RdKW20	20.450	2.590	0.05	0.013	Santos-Lopez et al. (2017)
pB1000	ColE1	*Haemophilus influenzae* RdKW20	25.020	1.920	0.054	0.002	Santos-Lopez et al. (2017)
pNI105		*Pseudomonas aeruginosa*	18.000	2.400	0.132	0.025	San Millan et al. (2014)
2-μM		*Saccharomyces cerevisiae*	52.000	0.000	0.0884	0.00416	Harrison et al. (2012)
pNUK73		*Pseudomonas aeruginosa*	11.030	1.890	0.214	0.008	San Millan et al. (2014)
pBGT	ColE1	*Escherichia coli*	19.120	1.560	0.057	0.013	San Millan et al. (2016)
pBGT R164S	ColE1	*Escherichia coli*	21.100	0.850	0.057	0.003	San Millan et al. (2016)
pBGT G54U	ColE1	*Escherichia coli*	44.500	3.810	0.207	0.019	San Millan et al. (2016)
pBGT G55U	ColE1	*Escherichia coli*	88.930	15.650	0.443	0.116	San Millan et al. (2016)
pBGT R164S G54U	ColE1	*Escherichia coli*	52.300	2.190	0.238	0.016	San Millan et al. (2016)
pBGT R164S G55U	ColE1	*Escherichia coli*	127.290	4.580	0.491	0.082	San Millan et al. (2016)

Abbreviation: SD, standard deviation.

PCN control is also an important feature of synthetic genetic circuits that use plasmids as vectors for the production of recombinant substances (Rouches et al., 2022).

To explore the interaction between the strength of selection and PCN, in this manuscript we postulated discrete-time and Wright–Fisher diffusion models with the following biological assumptions: (1) Plasmids encode for accessory genes that confer an advantage in harsh environments, for instance, antibiotic resistance genes; (2) bearing plasmids is associated with a fitness cost in the absence of selection for plasmid-encoded genes; (3) each plasmid segregates randomly to a daughter cell upon division; thus, plasmid-bearing bacteria can produce plasmid-free cells with a probability of $1/2^n$, where n is the PCN; (4) the cost associated with plasmid bearing is constant in time (no compensatory adaptation). We parameterized the model using a well-characterized multicopy plasmid, pBGT (Hernandez-Beltran et al., 2020; Rodriguez-Beltran et al., 2018; San Millan et al., 2016), and estimated the maximal growth rates of plasmid-bearing and plasmid-free cells by analyzing growth kinetics of each strain grown in isolation. From the growth curves, we obtained estimates for the fitness cost associated with plasmid bearing and the fitness advantage of the plasmid-bearing cells for a range of antibiotic concentrations. We also performed 1-day competition experiments between different subpopulations of PB and PF cells and evaluated how this fraction changed after a day of growth in media supplemented with antibiotics. Using this approach, we obtained theoretical and experimental iterative maps that we used to predict the long-term dynamics of the system.

Altogether, our results suggest that plasmid population dynamics in bacterial populations is predominantly driven by the existence of a trade-off between segregational loss and plasmid cost. We found that selection is necessary for the persistence of costly plasmids in the long term and that the strength of selection is highly correlated with the final fraction of plasmids in the entire population. As a result, whether plasmids are maintained or lost in the long term results from the complex interplay between PCN and its fitness cost, as well as the intensity and frequency of positive selection. As shown in the exhaustive exploration of parameters performed in this study, these relationships are highly nonlinear, thus resulting in the existence of an optimal PCN that depends on the rate of environmental fluctuation, the number of plasmids carried in each cell, and the fitness burden conferred by each plasmid-encoded gene in the absence of selection. In random environments, we observed a bimodal PCN* distribution, similar to the plasmid size distribution described for nontransmissible plasmids (Smillie et al., 2010) and for conjugative plasmids (Ledda & Ferretti, 2014).

Although both our theoretical and experimental models consider a multicopy plasmid with random segregation, the existence of an optimal PCN should also hold for nonrandom segregation (e.g., active partitioning), as this would decrease the probability of segregational loss (which corresponds to having a smaller value of μ_n in our model) so its optimal copy number will likely be lower than a plasmid that relies on random segregation (Lopez et al., 2021). By contrast, compensatory adaptation that reduces the fitness cost associated with plasmid bearing (in our model, a lower value of κ_n), would result in an increase in PCN*. We conclude by arguing that, as the existence of plasmids in natural environments requires intermittent periods of positive selection, the presence of plasmids contains information on the environment in which a population has evolved. Indeed, the plasmid copy number associates the frequency of selection with the energetic costs of plasmid maintenance. That is, there is a minimum frequency of drug exposure that allows multiple copies to persist in the population, and, for each environmental regime, there is an optimal number of plasmid copies.

AUTHOR CONTRIBUTIONS

J. Carlos R. Hernandez-Beltran: Conceptualization (equal); data curation (lead); formal analysis (equal); investigation (equal);

methodology (lead); software (lead); validation (lead); writing – original draft (equal); writing – review and editing (equal). **Verónica Miró Pina:** Conceptualization (equal); data curation (equal); formal analysis (lead); investigation (equal); methodology (lead); writing – original draft (equal); writing – review and editing (equal). **Arno Siri-Jégousse:** Conceptualization (equal); formal analysis (equal); investigation (equal); supervision (equal); writing – original draft (equal); writing – review and editing (equal). **Sandra Palau:** Conceptualization (equal); formal analysis (equal); investigation (equal); supervision (equal); writing – original draft (equal); writing – review and editing (equal). **Rafael Peña-Miller:** Conceptualization (equal); data curation (equal); formal analysis (equal); funding acquisition (lead); investigation (equal); methodology (equal); software (equal); supervision (lead); validation (lead); writing – original draft (lead); writing – review and editing (lead). **Adrián González Casanova:** Conceptualization (equal); formal analysis (equal); investigation (equal); supervision (equal); writing – original draft (equal); writing – review and editing (equal).

ACKNOWLEDGEMENTS

We thank A San Millan for the generous gift of the strains and for useful discussions. VMP acknowledges support of the Spanish Ministry of Science and Innovation to the EMBL partnership, the Centro de Excelencia Severo Ochoa and the CERCA Programme / Generalitat de Catalunya. VMP was also funded by the DGAPA-UNAM postdoctoral program. JCRHB was a doctoral student in Programa de Doctorado en Ciencias Biomédicas, Universidad Nacional Autónoma de México, and received fellowship 59691 from CONACYT. ASJ was supported by PAPIIT-UNAM (grant IA103820). RPM was supported by PAPIIT-UNAM (grant IN209419) and by CONACYT Ciencia Básica (grant A1-S-32164). AGC was supported by PAPIIT-UNAM (grant IN101722) and by CONACYT Ciencia Básica (grant A1-S-14615). The corresponding author was elected between the four PIs by means of a horse race where the winner horse was named Guilty Pleasure.

OPEN RESEARCH BADGES

This article has earned Open Data and Open Materials badges. Data and materials are available at https://doi.org/10.5281/zenodo.6360056.

DATA AVAILABILITY STATEMENT

The data and code underlying this article are available at: https://doi.org/10.5281/zenodo.6360056.

ORCID

J. Carlos R. Hernandez-Beltran https://orcid.org/0000-0003-4791-7206
Verónica Miró Pina https://orcid.org/0000-0001-6335-121X
Arno Siri-Jégousse https://orcid.org/0000-0003-1289-2950
Sandra Palau https://orcid.org/0000-0003-0986-6495
Rafael Peña-Miller https://orcid.org/0000-0002-2767-0640
Adrián González Casanova https://orcid.org/0000-0002-1744-6506

REFERENCES

Alonso, J. C., & Tolmasky, M. E. (2020). *Plasmids: Biology and impact in biotechnology and discovery*. John Wiley & Sons.

Alonso-del Valle, A., León-Sampedro, R., Rodríguez-Beltrán, J., DelaFuente, J., Hernández-García, M., Ruiz-Garbajosa, P., Cantón, R., Peña-Miller, R., & San Millán, A. (2021). Variability of plasmid fitness effects contributes to plasmid persistence in bacterial communities. *Nature Communications*, *12*, 1–14.

Ares-Arroyo, M., Coluzzi, C., & Rocha, E. P. (2022). Towards solving the conundrum of plasmid mobility: networks of functional dependencies shape plasmid transfer. *bioRxiv*. https://doi.org/10.1101/2022.07.04.498229

Athreya, K. B., & Ney, P. E. (2004). *Branching processes* (Vol. *1*). Dover Publications, Inc.

Baake, E., Casanova, A. G., Probst, S., & Wakolbinger, A. (2019). Modelling and simulating Lenski's long-term evolution experiment. *Theoretical Population Biology*, *127*, 58–74.

Baltrus, D. A. (2013). Exploring the costs of horizontal gene transfer. *Trends in Ecology & Evolution*, *28*, 489–495.

Bergstrom, C. T., Lipsitch, M., & Levin, B. R. (2000). Natural selection, infectious transfer and the existence conditions for bacterial plasmids. *Genetics*, *155*, 1505–1519.

Chen, I., & Dubnau, D. (2004). DNA uptake during bacterial transformation. *Nature Reviews Microbiology*, *2*, 241–249.

Chen, J., Quiles-Puchalt, N., Chiang, Y. N., Bacigalupe, R., Fillol-Salom, A., Chee, M. S. J., Fitzgerald, J. R., & Penadés, J. R. (2018). Genome hypermobility by lateral transduction. *Science*, *362*, 207–212.

Chevin, L.-M. (2011). On measuring selection in experimental evolution. *Biology Letters*, *7*, 210–213.

Del Solar, G., & Espinosa, M. (2000). Plasmid copy number control: An ever-growing story. *Molecular Microbiology*, *37*, 492–500.

Dimitriu, T., Matthews, A. C., & Buckling, A. (2021). Increased copy number couples the evolution of plasmid horizontal transmission and plasmid-encoded antibiotic resistance. *Proceedings of the National Academy of Sciences of the United States of America*, *118*, e2107818118.

Dykhuizen, D. E. (1990). Experimental studies of natural selection in bacteria. *Annual Review of Ecology and Systematics*, *21*, 373–398.

Etheridge, A. (2011). *Some mathematical models from population genetics: École D'Été de probabilités de Saint-Flour XXXIX-2009* (Vol. *2012*). Springer Science & Business Media.

Funnell, B. E., & Phillips, G. (2004). *Plasmid biology* (Vol. *672*). ASM Press.

Garoña, A., Hülter, N. F., Romero Picazo, D., & Dagan, T. (2021). Segregational drift constrains the evolutionary rate of prokaryotic plasmids. *Molecular Biology and Evolution*, *38*, 5610–5624.

Gerrish, P., & Lenski, R. (1998). The fate of competing beneficial mutations in an asexual population. *Genetica*, *102*, 127–144.

González Casanova, A., Kurt, N., Wakolbinger, A., & Yuan, L. (2016). An individual-based model for the Lenski experiment, and the deceleration of the relative fitness. *Stochastic Processes and their Applications*, *126*, 2211–2252.

Greenfield, B. K., Shaked, S., Marrs, C. F., Nelson, P., Raxter, I., Xi, C., McKone, T. E., & Jolliet, O. (2018). Modeling the emergence of antibiotic resistance in the environment: An analytical solution for the minimum selection concentration. *Antimicrobial Agents and Chemotherapy*, *62*, e01686-17.

Groisman, E. A., & Ochman, H. (1996). Pathogenicity islands: Bacterial evolution in quantum leaps. *Cell*, *87*, 791–794.

Gullberg, E., Cao, S., Berg, O. G., Ilbäck, C., Sandegren, L., Hughes, D., & Andersson, D. I. (2011). Selection of resistant bacteria at very low antibiotic concentrations. *PLoS Pathogens*, *7*, e1002158.

Hall, B. G., Acar, H., Nandipati, A., & Barlow, M. (2014). Growth rates made easy. *Molecular Biology and Evolution*, *31*, 232–238.

Hall, J. P., Wood, A. J., Harrison, E., & Brockhurst, M. A. (2016). Source–sink plasmid transfer dynamics maintain gene mobility in soil bacterial communities. *Proceedings of the National Academy of Sciences of the United States of America*, *113*, 8260–8265.

Harrison, E., Koufopanou, V., Burt, A., & Maclean, R. (2012). The cost of copy number in a selfish genetic element: The 2-μm plasmid of *Saccharomyces cerevisiae*. *Journal of Evolutionary Biology*, *25*, 2348–2356.

Hernandez-Beltran, J., Rodríguez-Beltrán, J., Aguilar-Luviano, B., Velez-Santiago, J., Mondragón-Palomino, O., MacLean, R. C., Fuentes-Hernández, A., Millán, A. S., & Peña-Miller, R. (2022). Antibiotic heteroresistance generated by multi-copy plasmids. *bioRxiv*. https://doi.org/10.1101/2022.08.24.505173

Hernandez-Beltran, J., Rodríguez-Beltrán, J., San Millán, A., Peña-Miller, R., & Fuentes-Hernández, A. (2020). Quantifying plasmid dynamics using single-cell microfluidics and image bioinformatics. *Plasmid*, *113*, 102517.

Ilhan, J., Kupczok, A., Woehle, C., Wein, T., Hülter, N. F., Rosenstiel, P., Landan, G., Mizrahi, I., & Dagan, T. (2019). Segregational drift and the interplay between plasmid copy number and evolvability. *Molecular Biology and Evolution*, *36*, 472–486.

Jahn, M., Vorpahl, C., Hübschmann, T., Harms, H., & Müller, S. (2016). Copy number variability of expression plasmids determined by cell sorting and droplet digital pcr. *Microbial Cell Factories*, *15*, 1–12.

Kumar, P., Maschke, H., Friehs, K., & Schügerl, K. (1991). Strategies for improving plasmid stability in genetically modified bacteria in bioreactors. *Trends in Biotechnology*, *9*, 279–284.

Kussell, E., & Leibler, S. (2005). Phenotypic diversity, population growth, and information in fluctuating environments. *Science*, *309*, 2075–2078.

Ledda, A., & Ferretti, L. (2014). A simple model for the distribution of plasmid lengths. *arXiv*. https://doi.org/10.48550/arXiv.1411.0297

Lopez, J., Donia, M., & Wingreen, N. (2021). Modeling the ecology of parasitic plasmids. *The ISME Journal*, *15*, 2843–2852.

Million-Weaver, S., Alexander, D. L., Allen, J. M., & Camps, M. (2012). Quantifying plasmid copy number to investigate plasmid dosage effects associated with directed protein evolution. *Methods in Molecular Biology (Clifton, N.J.)*, *834*, 33–48. https://doi.org/10.1007/978-1-61779-483-4_3

Mochizuki, A., Yahara, K., Kobayashi, I., & Iwasa, Y. (2006). Genetic addiction: Selfish gene's strategy for symbiosis in the genome. *Genetics*, *172*, 1309–1323.

Münch, K., Münch, R., Biedendieck, R., Jahn, D., & Müller, J. (2019). Evolutionary model for the unequal segregation of high copy plasmids. *PLoS Computational Biology*, *15*, 1–17.

Paulsson, J. (2002). Multileveled selection on plasmid replication. *Genetics*, *161*, 1373–1384.

Paulsson, J., & Ehrenberg, M. (1998). Trade-off between segregational stability and metabolic burden: A mathematical model of plasmid cole1 replication control. *Journal of Molecular Biology*, *279*, 73–88.

Pemberton, J., & Don, R. (1981). Bacterial plasmids of agricultural and environmental importance. *Agriculture and Environment*, *6*, 23–32.

Petzoldt, T. (2019). *Estimate growth rates from experimental data*. R package version 0.8.1. https://CRAN.R-project.org/package=growthrates

R Core Team. (2020). *R: A language and environment for statistical computing*. R Foundation for Statistical Computing https://www.R-project.org

Raj, A., & van Oudenaarden, A. (2008). Nature, nurture, or chance: Stochastic gene expression and its consequences. *Cell*, *135*, 216–226.

Rodríguez-Beltrán, J., DelaFuente, J., León-Sampedro, R., MacLean, R. C., & San Millán, Á. (2021). Beyond horizontal gene transfer: The role of plasmids in bacterial evolution. *Nature Reviews Microbiology*, *19*, 347–359.

Rodriguez-Beltran, J., Hernandez-Beltran, J. C. R., DelaFuente, J., Escudero, J. A., Fuentes-Hernandez, A., MacLean, R. C., Peña-Miller, R., & San Millan, A. (2018). Multicopy plasmids allow bacteria to escape from fitness trade-offs during evolutionary innovation. *Nature Ecology & Evolution*, *2*, 873–881.

Rodriguez-Beltran, J., Sørum, V., Toll-Riera, M., de la Vega, C., Peña-Miller, R., & Millán, A. S. (2019). Genetic dominance governs the evolution and spread of mobile genetic elements in bacteria. *bioRxiv*. https://doi.org/10.1101/863472

Rouches, M. V., Xu, Y., Cortes, L. B. G., & Lambert, G. (2022). A plasmid system with tunable copy number. *Nature Communications*, *13*, 1–12.

Salje, J. (2010). Plasmid segregation: How to survive as an extra piece of DNA. *Critical Reviews in Biochemistry and Molecular Biology*, *45*, 296–317.

Salverda, M. L., De Visser, J. A. G., & Barlow, M. (2010). Natural evolution of tem-1 β-lactamase: Experimental reconstruction and clinical relevance. *FEMS Microbiology Reviews*, *34*, 1015–1036.

San Millan, A. (2018). Evolution of plasmid-mediated antibiotic resistance in the clinical context. *Trends in Microbiology*, *26*, 978–985.

San Millan, A., Escudero, J. A., Gifford, D. R., Mazel, D., & MacLean, R. C. (2016). Multicopy plasmids potentiate the evolution of antibiotic resistance in bacteria. *Nature Ecology & Evolution*, *1*, 1–8.

San Millan, A., Heilbron, K., & MacLean, R. C. (2014). Positive epistasis between co-infecting plasmids promotes plasmid survival in bacterial populations. *The ISME Journal*, *8*, 601–612.

San Millan, A., & Maclean, R. C. (2017). Fitness costs of plasmids: A limit to plasmid transmission. *Microbiology Spectrum*, *5*, 5.5.02.

Santer, M., & Uecker, H. (2020). Evolutionary rescue and drug resistance on multicopy plasmids. *Genetics*, *215*, 847–868.

Santos-Lopez, A., Bernabe-Balas, C., Millan, A. S., Ortega-Huedo, R., Hoefer, A., Ares-Arroyo, M., & Gonzalez-Zorn, B. (2017). Compensatory evolution facilitates the acquisition of multiple plasmids in bacteria. *bioRxiv*. https://doi.org/10.1101/187070

Smillie, C., Garcillán-Barcia, M. P., Francia, M. V., Rocha, E. P., & de la Cruz, F. (2010). Mobility of plasmids. *Microbiology and Molecular Biology Reviews*, *74*, 434–452.

Stevenson, C., Hall, J. P., Brockhurst, M. A., & Harrison, E. (2018). Plasmid stability is enhanced by higher-frequency pulses of positive selection. *Proceedings of the Royal Society B: Biological Sciences*, *285*, 20172497.

Stewart, F. M., & Levin, B. R. (1977). The population biology of bacterial plasmids: A priori conditions for the existence of conjugationally transmitted factors. *Genetics*, *87*, 209–228.

Vogwill, T., & MacLean, R. C. (2015). The genetic basis of the fitness costs of antimicrobial resistance: A meta-analysis approach. *Evolutionary Applications*, *8*, 284–295.

Yurtsev, E. A., Chao, H. X., Datta, M. S., Artemova, T., & Gore, J. (2013). Bacterial cheating drives the population dynamics of cooperative antibiotic resistance plasmids. *Molecular Systems Biology*, *9*, 683.

How to cite this article: Hernandez-Beltran, J. C. R., Miró Pina, V., Siri-Jégousse, A., Palau, S., Peña-Miller, R., & González Casanova, A. (2022). Segregational instability of multicopy plasmids: A population genetics approach. *Ecology and Evolution*, *12*, e9469. https://doi.org/10.1002/ece3.9469

APPENDIX A

Experimental methods

BACTERIAL STRAINS AND MEDIA

The plasmid-free strain we used was *E. coli* K12 MG1655 and the plasmid-bearing strain was MG/pBGT carrying the multicopy plasmid pBGT with the β-lactamase $bla_{\text{TEM-1}}$, which confers resistance to ampicillin and the fluorescent protein GFP under an arabinose-inducible promoter. Mean plasmid copy number in the population is PCN = 19.1 ± 3.8 (San Millan et al., 2016). Overnight cultures were grown in flasks with 20 ml of lysogeny broth (LB; Sigma L3022) with 0.5% w/v L-(+)-Arabinose (Sigma A91906) for fluorescence induction, in a shaker-incubator at 220 RPM at 37°C. For the plasmid-bearing strain, 25 mg/L of ampicillin (Sigma A0166) was added to eliminate segregant cells. Ampicillin stock solutions were prepared at 100 mg/ml directly in LB and sterilized by 0.22 μm (Millex-GS SLGS033SB) filtering. Arabinose stock solutions were prepared at 20% w/v in DD water and sterilized by filtration.

BACTERIAL GROWTH EXPERIMENTS

Growth kinetics measurements of each strain were performed in 96-well plates with 200 μl of LB with 0.5% w/v arabinose without antibiotics, plates were sealed using X-Pierce film (Sigma Z722529), and each well seal film was pierced in the middle with a sterile needle to avoid condensation. Plates were grown at 37°C, and readings for OD and fluorescence were made every 20 min in a fluorescence microplate reader (BioTek Synergy H1), after 30-s linear shaking.

COMPETITION EXPERIMENTS

Competition experiments were performed using 96-well plates with 200 μl of LB with 0.5% w/v arabinose, and respective ampicillin concentrations: 0, 1, 2, 2.5, 3, 3.5, 4, and 6 mg/L were implemented by plate rows. To construct our inoculation plate, overnight cultures of the plasmid-free strain and the plasmid-bearing strain were adjusted to an OD of 1 (630 nm) using a BioTek ELx808 Absorbance Microplate Reader diluted with fresh ice-cooled LB. Appropriate volumes were mixed to make co-cultures at fractions 0, 0.1, 0.2,..., 1 and set column-wise on a 96-well plate (Corning CLS3370). We then used a 96-pin microplate replicator (Boekel 140500) with flame sterilization before each inoculation. Four replicates plates were grown in static incubator at 37°C. After 24-h growth, plates were read in a fluorescence microplate reader (BioTek Synergy H1) using OD (630 nm) and eGFP (479,520 nm) after 1 min of linear shaking.

PLASMID FRACTION DETERMINATION

To calculate the fluorescence intensity, we first subtracted the background signal of LB for fluorescence and OD, respectively, and then the debackgrounded the fluorescence signal was scaled by dividing by the debackgrounded OD. The measurements for our inoculation plate showed a strong linear correlation (R^2 = .995) between co-cultures fractions and fluorescence intensity (Figure 3b). This allowed to directly approximate the population's plasmid fractions from the readings of our competition experiments. We normalized the data independently for each antibiotic concentration taking the average measurements of the four replicates. Plasmid fractions, *PF*, were inferred by normalizing the mean fluorescence intensity for each well, f_i, to the interval [0,1] using the following formula: $PF_i = (f_i - f_{\min})/(f_{\max} - f_{\min})$ were $f_{\max}$ and $f_{\min}$ are the mean fluorescence intensities at fractions 1 and 0, respectively.

APPENDIX B

Mathematical model

FIXED POINTS OF EQUATION (2)

Let $\bar{f} = f \circ g$. We want to study the fixed points of $\bar{f}$ and their domains of attraction. It is not hard to see that 0 is always fixed point, and once the frequency reaches 0, it stays at 0. In addition, if $x \neq 0$,

$$\begin{aligned}\bar{f}(x) &= \frac{x(1-\kappa_n)(1-\mu_n)/(\alpha-\kappa_n)}{(1-\alpha)/(\alpha-\kappa_n)+x} = x \\ \Leftrightarrow x^2 + \frac{1-\alpha}{\alpha-\kappa_n}x &= \frac{(1-\kappa_n)(1-\mu_n)}{\alpha-\kappa_n}x \\ \Leftrightarrow x &= \frac{(1-\kappa_n)(1-\mu_n)-(1-\alpha)}{\alpha-\kappa_n} = 1-\mu_n\frac{1-\kappa_n}{\alpha-\kappa_n}.\end{aligned}$$

Denote $x^* := 1 - \mu_n(1-\kappa_n)/(\alpha-\kappa_n)$. Since the frequencies are in [0,1], this fixed point only exists if $\alpha > \kappa_n + \mu_n(1-\kappa_n)$. As n increases, μ_n decreases exponentially, while κ_n increases only linearly, so there is a nonlinear relationship between n and the minimum α required for the existence of a second fixed point x^*.

Let us analyze the stability of x^*. Let us assume that $\alpha > \kappa_n + \mu_n(1-\kappa_n)$.

$$\begin{aligned}\bar{f}(x) - x &= \frac{x(1-\kappa_n)(1-\mu_n)/(\alpha-\kappa_n) - x(1-\alpha)/(\alpha-\kappa_n) - x^2}{(1-\alpha)/(\alpha-\kappa_n)+x} > 0 \\ \Leftrightarrow \frac{(1-\kappa_n)(1-\mu_n)}{(\alpha-\kappa_n)} &- \frac{1-\alpha}{\alpha-\kappa_n} - x > 0 \\ \Leftrightarrow x &< x^*.\end{aligned}$$

So, the frequency increases if it is below x^* and decreases otherwise, meaning that it is a stable fixed point. In addition, the domain of attraction is (0,1], meaning that this equilibrium fraction is reached for any initial state.

To sum up, 0 is always a fixed point. If $\alpha > \kappa_n + \mu_n(1-\kappa_n)$, then there is an additional stable fixed points x^*.

CHOICE OF THE MODEL

In this section, we compare two types of mathematical models for the evolution of plasmid-bearing frequencies, the discrete-time model used in this paper (Equation (2)) and the Wright–Fisher diffusion.

There had been several attempts to adapt the classical theory of Wright–Fisher models to this experimental setting (see for example (Chevin, 2011)). A mathematical rigorous way to do this was developed in González Casanova et al. (2016). In Gerrish & Lenski (1998)

a heuristic and applicable to data framework was introduced. Recently, in Baake et al. (2019), the two methodologies had been paired in order to have a rigorous and applicable way to use classic population genetics to study evolutionary experiments. In this work, days take the role of generations, and as the number of individuals after each sampling is more or less constant, the assumption of constant population size becomes reasonable.

Let us assume that the mutation rate $\mu_{N,n} = 2^{-n}$ and the cost $\kappa_{N,n}$ are parameterized by N. To see the accumulated effects of plasmid costs, segregational loss, and genetic drift, we need $\kappa_{N,n}$ and $\mu_{N,n}$ to be of order $1/N$ (see, e.g., Chapter 5 in Etheridge, 2011). The first condition is fulfilled if the cost per plasmid is very low, for example, when $\kappa_{N,n} = \kappa n/N$. The second one stands if n is of order $\log_2(N)$, which is the case, for example, if $n = 20$ and $N = 10$ (Pemberton & Don, 1981), or if $n = 15$ and $N = 10$ (Alonso & Tolmasky, 2020). In that case, we set $\mu = N2^{-n}$. Under this setting, when time is accelerated by N, the frequency process of individuals with plasmids can be approximated by the solution of the stochastic differential equation (SDE).

$$dX_t = -\mu X_t dt - \kappa X_t(1 - X_t)dt + \sqrt{X_t(1 - X_t)}dB_t, \tag{5}$$

where B is a standard Brownian motion. This is known as the Wright–Fisher diffusion with mutation and selection. When antibiotic is added, at times $\{T,2T,\ldots\}$, then (5) modifies to

$$dX_t = \sum_{j\geq 1} \frac{\alpha X_{jT-}(1 - X_{jT-})}{1 - \alpha(1 - X_{jT-})} \mathbf{1}_{jT\leq t} - \mu X_t dt - \kappa X_t(1 - X_t)dt + \sqrt{X_t(1 - X_t)}dB_t. \tag{6}$$

However, in our experimental setting, the cost that we measure ($\kappa_n \simeq 0.27$) is much higher than the inverse population size, so we are in the regime of strong selection. In other words, for plasmids that have a very small cost, of the order of $1/N$, genetic drift would play an important role, and the above Wright–Fisher diffusion with mutation, selection and antibiotic peaks (6) would be the most suitable model. But in our setting, selection (plasmid costs) is so high that genetic drift becomes negligible. Recall that Equation (2) does not need any time rescaling, whereas in the diffusion (6) time is measured in units of N generations. Under strong selection, the frequencies evolve much faster.

APPENDIX C

Numerical simulations

COMPUTER IMPLEMENTATION

The model was implemented in Python, using standard scientific computing libraries (Numpy, MatplotLib, and the Decimal library were required to resolve small numbers conflicts). In general, all simulations started at PB frequency 1 (unless stated otherwise). Numeric simulations were defined to reach a steady state when values first repeat. In the case of periodic environments, the repetition must happen at antibiotic peak days. We considered extinction if the end point of the realization dropped below a threshold adjusted to the simulations times, the highest being 1×10^{-7} and the lowest 1×10^{-100}.

RANDOM ENVIRONMENTS

Environmental sequences of size 1000 (days) using a binomial distribution varying the probability of success. For each environment created, we also bit-flipped (so 101... turns into 010...) and two measures were applied to each resulting environment. First, we used Shannon entropy, $H(Env) = -\sum_i^n p_i log_n(p_i)$, with two states, $n = 2$ (antibiotic or no-antibiotic) and p_i equal to the probability of finding a state day, that is, the fractions of days with antibiotics and without antibiotics. We classified environments by their H and by the fraction of antibiotic days, as being this an important feature. These two measures are in the [0,1] interval, so we binned the intervals into 20 bins and 1000 environments were created for each bin.

MODEL PARAMETRIZATION

Growth kinetics parameters were estimated using the R (R Core Team, 2020) package growth rates (Petzoldt, 2019). Exponential phase duration, σ, was calculated by finding lag phase duration and the time to reach carrying capacity using the nonlinear growth model Baranyi. Maximum growth rates, r and $r+\rho_n$, were estimated using the nonparametric smoothing splines method. κ_n value was estimated using Equation (1) and the data from the antibiotic-free competition experiment using a curve fitting algorithm from the SciPy library in a custom Python script. Respective values of α were found in the same manner using Equation (2) and fixing κ_n. κ_n was also calculated using the formula in Equation (4) with a very similar result. The parameters are summarized in Tables 1 and 2.